



8-2017

Design of a Robotic Instrument Manipulator for Endoscopic Deployment

Ryan Ponten

University of Tennessee, Knoxville, rponten@vols.utk.edu

Recommended Citation

Ponten, Ryan, "Design of a Robotic Instrument Manipulator for Endoscopic Deployment. " Master's Thesis, University of Tennessee, 2017.

https://trace.tennessee.edu/utk_gradthes/4921

This Thesis is brought to you for free and open access by the Graduate School at Trace: Tennessee Research and Creative Exchange. It has been accepted for inclusion in Masters Theses by an authorized administrator of Trace: Tennessee Research and Creative Exchange. For more information, please contact trace@utk.edu.

To the Graduate Council:

I am submitting herewith a thesis written by Ryan Ponten entitled "Design of a Robotic Instrument Manipulator for Endoscopic Deployment." I have examined the final electronic copy of this thesis for form and content and recommend that it be accepted in partial fulfillment of the requirements for the degree of Master of Science, with a major in Mechanical Engineering.

Daniel C. Rucker, Major Professor

We have read this thesis and recommend its acceptance:

William Hamel, Jindong Tan

Accepted for the Council:

Dixie L. Thompson

Vice Provost and Dean of the Graduate School

(Original signatures are on file with official student records.)

Design of a Robotic Instrument Manipulator for Endoscopic Deployment

A Thesis Presented for the
Master of Science
Degree

The University of Tennessee, Knoxville

Ryan Ponten

August 2017

© by Ryan Ponten, 2017
All Rights Reserved.

*To my love Kristine,
my closest friend and partner in everything.
You made this possible.*

Acknowledgments

I would first like to thank my advisory committee which includes Caleb Rucker, Bill Hamel, and Jindong Tan, for reviewing my work and encouraging the development of this thesis.

I would also like to thank the group at the REACH Lab who worked alongside me and created a stimulating and enjoyable lab environment. Early on, I primarily worked with Caroline Black towards the development of the endoscopic instrument project and her design analysis work on the concentric-tube robot contributed to much of Chapter 2. Kaitlin Oliver-Butler’s work on the CAAR project supported similar design analysis, and I also greatly benefited from her manufacturing and prototyping knowledge. I give a lot of credit to John Till for dependably answering any and all questions I had about mechanics modeling or coding, especially because I *always* had questions. Vince Aloï assisted with the bending experiments performed on the colonoscope, and his efforts support the work presented in Chapter 3. Several undergraduate researchers also had a role in this thesis work, including Andrew Orekhov, James Ferguson, Dylan Hoskins, Grant Given, and Liam Page.

Additionally, I want to thank my advisor Caleb Rucker for inviting me to be a part of the REACH Lab. I had not previously considered research as a possibility for my career, but his passion for educating students and fostering new ideas was a much-needed reminder of everything I enjoy about engineering. At the lab, we benefit daily from his mentorship and constant willingness to ponder difficult problems alongside us.

Lastly, I want to express my deep gratitude and love for my wife Kristine, who provided unending support throughout this process. I am incredibly blessed to be her partner in life, and I will always remember how much she encouraged me to pursue what I enjoy. I am excited about our next steps together and what the next adventure may bring.

Abstract

This thesis describes the initial design process for an application of continuum robotics to endoscopic surgical procedures, specifically dissection of the colon. We first introduce the long-term vision for a benchtop dual-instrument endoscopic system with intuitive haptic controllers and then narrow our focus to the design and testing of the instrument manipulator itself, which must be actuated through the long, winding channel of a standard colonoscope.

Based on design requirements for a target procedure, we analyze simulations of two types of continuum robots using recently established kinematic and mechanic modeling approaches: the concentric-tube robot (CTR) and the concentric agonist-antagonist robot (CAAR). In addition, we investigate solutions to the primary engineering challenge to this system, which is accurately transmitting joint motion through flexible, hollow shafts. Based on our study of the manipulator simulations and transmission shafts, we select instrument designs for prototyping and testing. We present approaches for controlling the position of the robotic instrument in real-time using an input device, and demonstrate the degree of control we can achieve in various configurations by performing time trial experiments with our prototype robotic instruments. Our observations of the manipulator during testing inform us of sources of error, and we conclude this report with suggestions for future work, including shaft design and alternative continuum manipulator approaches.

Table of Contents

1	Background & Motivation	1
1.1	Existing Medical Robots	1
1.2	Research Trend: Continuum Robotics	2
1.3	Description of Purpose	2
1.4	Design Specifications	4
2	Manipulator Design	7
2.1	Concentric-Tube Robots	7
2.1.1	Overlap Constraint	8
2.2	CTR Modeling	9
2.2.1	Kinematics Overview	11
2.2.2	Jacobian Discontinuities	12
2.3	Concentric Agonist-Antagonist Robots	15
2.4	CAAR Modeling	16
2.5	Manipulator Simulation Analysis	18
2.5.1	CTR Workspace	18
2.5.2	CAAR Workspace	20
2.5.3	Resolution Analysis	21
2.6	Discussion	24
3	Transmission Design	25
3.1	Colonoscope Constraints	27
3.1.1	Colonoscope Bending Test	27

3.1.2	Transmission Requirements	28
3.2	Candidate Transmission Designs	28
3.2.1	Notched Transmission Approach	28
3.2.2	FDM Printed Tube	30
3.2.3	Purchased Tubes	30
3.3	Performance	33
4	Prototyping & Testing	34
4.1	Manipulator Prototyping	34
4.2	Actuation System Design	35
4.3	CAAR vs. CTR	37
4.4	Real-Time Control	38
4.4.1	Low-Level Motion Commands	38
4.4.2	Position Control Approaches	39
4.5	Results	41
5	Conclusions & Future Work	46
	Bibliography	48
	Vita	54

List of Tables

1.1	Endoscopic instrument design specifications	5
2.1	Concentric tube kinematic variables	10
2.2	Parameters of example CTR design	18
2.3	Parameters of example CAAR design	21
3.1	Colonoscope bending test results	27
3.2	Transmission design requirements	28
3.3	Transmission design results	32
4.1	Time trial results, no transmission	42
4.2	Time trial results with colonoscope deployment	44

List of Figures

1.1	Continuum Robots	3
1.2	System overview	5
2.1	Concentric-tube robot basics	8
2.2	Preliminary benchtop system design	9
2.3	CTR transition overlap	12
2.4	CTR end effector discontinuous motion	13
2.5	CAAR bending motion	15
2.6	CAAR geometry	16
2.7	CTR workspace simulation	19
2.8	CAAR workspace simulation	20
2.9	CTR spatial resolution simulation	22
2.10	CAAR spatial resolution simulation	23
3.1	Colonoscope entry port	26
3.2	Colonoscope flexural rigidity	26
3.3	Notched stainless steel tube model	29
3.4	3D-printed transmission	30
3.5	Purchased transmission tubing	31
3.6	Surgical grasper	32
4.1	CTR prototype	34
4.2	Initial CAAR prototype concepts	35
4.3	Final CAAR prototype	36

4.4	Actuation system	37
4.5	Control diagram	38
4.6	Joint space motion	41
4.7	Position control experiment	42
4.8	Surgical training task experiment	43
4.9	Endoscopic deployment test, straightened transmission	45

Chapter 1

Background & Motivation

1.1 Existing Medical Robots

Over the last 20 years, the use of robots to assist surgical procedures has increased rapidly. The advancements made in actuation, instrumentation, processing power, and materials have allowed surgical robots to be designed with greater positioning accuracy and dexterity. Additionally, there has been an increase in surgeon acceptance of robotic tools, especially as more intuitive controls and input devices are integrated with robot manipulation.

No single robot has had a greater impact on the growth of medical robotics than the Da Vinci system by Intuitive Surgical [17]. Initially designed for laparoscopy, the Da Vinci system is now available in several models and is cleared for many procedures. It is the only system with over a thousand installations worldwide and has been studied in over 10,000 peer-reviewed publications [29]. Although the Da Vinci has been proven capable in many procedures, the recent rise of research into robot-assisted surgery has driven the development of a diverse set of robots, many of which are designed for specific procedures. Other examples of successful surgical robots include the Pathfinder and the Renaissance for neurosurgery [12] [18], the Sensei X for catheter positioning [24], and many others. Each of these robots has improved the performance and increased the occurrence of minimally invasive surgery (MIS), which has become a foundational source of research in the field of medical robotics. It has been shown to reduce hospital time, cost, and patient trauma. The continuation of

robotics research can improve the accuracy and control aspects of existing minimally invasive procedures, as well as open up possibilities of new and previously impossible procedures.

1.2 Research Trend: Continuum Robotics

The work presented in this thesis falls within the specific research trend of continuum robotics for surgical procedures. While traditional robot structures have enabled better performance in many procedures, it has recently been of great interest to explore the capabilities of continuously flexible manipulators for reaching surgical sites in the body that are difficult to access. Robots with these type of structures can conform to curved paths and can easily be miniaturized to fit through small access ports. This allows natural orifices in the body to become a feasible alternative for tool entry, and reduces the need for invasive approaches. As discussed in a recent survey by Burgner-Kahrs et. al, several examples of continuum robot systems have been developed that demonstrate unique aptitude for many procedures located in remote areas of the body [5].

As shown in Figure 1.1, a variety of tasks can be accomplished using continuum manipulators. Although many continuum robotic systems have been developed, all of them share similar mechanical characteristics because of the necessity of highly elastic members that contribute to overall robot flexibility. In recent years, researchers have developed mathematical modeling and control techniques that enable accurate manipulation of soft robot structures. This progress has enabled successful surgical verification experiments that raised awareness of the high potential of continuum robots for surgery. In this thesis, we seek to apply continuum robotics to one of the more difficult to access workspaces in the human body, the colon. In the following section, we highlight the importance of minimally invasive surgery for endoscopic procedures and define the overarching goal of the study.

1.3 Description of Purpose

This year, thousands of Americans diagnosed with colorectal cancer will need surgery to dissect and potentially resect portions of the colon. Minimally invasive surgical techniques

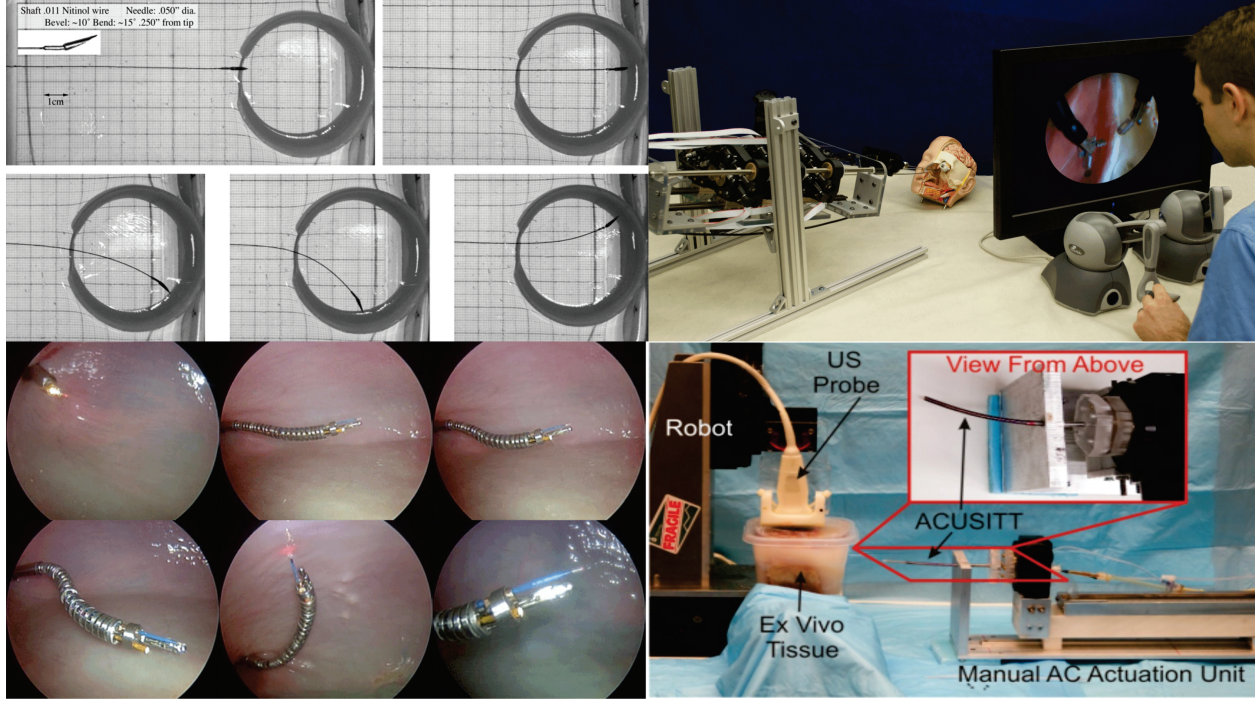


Figure 1.1: Continuum robots in surgery: (**Top Left**) Engh et al. utilize duty-cycle spinning of a bevel-tipped needle to achieve nonlinear trajectories [7]. (**Top Right**) Burgner et al. teleoperate a concentric-tube manipulator during a realistic surgical scenario [4]. (**Bottom Left**) Goldman et al. designed a telerobotic system for transurethral surveillance and surgical intervention using a flexible manipulator [8]. (**Bottom Right**) Burdette et al. perform an ex vivo liver ablation experiment using a steerable needle device [3].

have demonstrated equivalent oncologic outcomes with significantly reduced postoperative complications. However, this still requires major intra-abdominal surgery. Laparoscopic techniques are not easily adaptable to the cylindrical workspace of the colon. In order for patients and surgeons to maximize the benefits of MIS, technological advances in flexible manipulation are required to enhance currently used endoscopic surgical tools. Our goal is to provide these advances with flexible robotic tool manipulators to enhance the dexterity and strength of current tools while providing intuitive control and maximizing visualization with smaller manipulators.

While some early (T1) rectal cancers near the anal verge can be removed with laparoscopic instruments passed through the anus or introduced via the abdomen, and small, pre-invasive polyps and lesions can be treated with endoscopic mucosal resection (EMR) during colonoscopy, as colorectal tumors grow larger and deeper into the submucosa, the surgical

procedure becomes more difficult and time consuming. Colonic endoscopic submucosal dissection (ESD) is difficult due to the thin walls, narrow lumen, acute angulations in the colon [36], and inherent risk of perforation. ESD can potentially further minimize operative risks for patients by removing the need for colon resection for pre-malignant polyps [14]. However, its widespread practice has been hindered by the difficulty of manipulating dissection tools endoscopically [15] and the subsequent risks due to this difficulty.

Patients with advanced colorectal cancer require full-thickness resection. Currently, this procedure requires either an open (for large sections) or laparoscopic (for smaller sections) approach to repair the opening in the colon wall. Laparoscopic colorectal surgery reduces postoperative complications, yet still carries with it a hospital mortality of 1%, anastomotic leak of up to 10%, and conversion to open surgery of 18% [36]. Therefore, surgeons are exploring an endoscopic approach to pre-malignant colorectal neoplasms called endoscopic full-thickness resection (EFTR) [11, 22, 28]. A safe and reliable endoscopic system that can perform full-thickness resection would allow surgeons to remove potentially pre-malignant tissue when lab testing is unclear or unachievable in order to avoid additional operations and local recurrences [23]. Reviews of EFTR have been mixed, and the consensus is that the technique of EFTR is developing, but the inability to close the resection defect reliably is a major obstacle [1].

Our overarching hypothesis is that a robot-assisted endoscopic tool manipulation system can reduce difficulty, risk, and procedure time for colorectal tumor resection and decrease the number of invasive procedures required for large section tissue removal. In the following section (1.4), we first define basic design requirements for an endoscopic instrument. We then explore the suitability of two types of continuum robotic structures in Chapter 2. Both of these robots require rotary actuation, and in Chapter 3, we describe the challenge of transmitting rotation through an endoscope and investigate various solutions.

1.4 Design Specifications

Through a literature review of procedure requirements and discussion with experienced surgeons, we have established (1) a desired workspace, (2) size constraints on the instrument

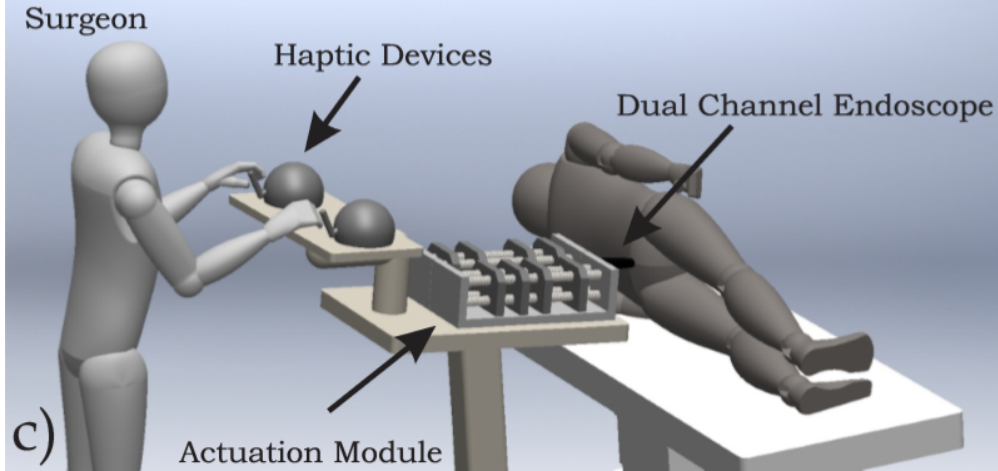


Figure 1.2: Benchtop robotic instrument system mockup

manipulators such that they can be deployed through tool-port channels in currently available colonoscopes and allow standard tools to pass through the lumen, and (3) an accuracy requirement for effective surgical teleoperation. These parameters have been organized in Table 1.1.

The established specifications are used throughout this study to evaluate the suitability of several instrument manipulator designs. These values are baseline goals, and as demonstrated in later stages of this endeavor, we discover additional design requirements that may be specific to each type of manipulator (e.g. torsion minimization in the CTR via overlap constraints). We also develop design restrictions through information gained from testing physical prototypes. However, the basic parameters organized in Table 1.1 allow us to take first steps in manipulator design. Figure 1.2 illustrates the long-term system goal for

Table 1.1: Table of design specifications for instrument

Specification	Value
Workspace Volume	(Cylinder) Diameter: 4-6 cm, Length: 8-10 cm [13]
Working Channel Size	Diameter: 2.8 and 3.8 mm [31]
Maximum tool size	Diameter 1.9 mm
Accuracy	< 1 mm [9]

the benchtop robotic instrument manipulator. The scope of the work presented here does not include integration of haptic feedback or dual-channel instruments, but we hope that the findings will support the development of such a system.

Chapter 2

Manipulator Design

In the following sections, two types of continuum robots are considered for endoscopic deployment: the concentric-tube robot (CTR) and the concentric agonist-antagonist robot (CAAR). We first introduce the concept and kinematics of each type of robot and discuss their unique characteristics. We conclude the chapter with analysis of manipulator workspace and resolution in either case, providing insight into necessary design features for successful endoscopic deployment.

2.1 Concentric-Tube Robots

As shown in Figure 2.1, concentric-tube robots consist of multiple precurved elastic tubes that are arranged concentrically. The base of each tube is independently axially rotated and translated by an actuation system in order to change the distal shape of the tube collection and control the pose of the tip. Recently, concentric-tube manipulators have been developed for several surgical procedures, such as cardiac [27], transnasal [33], and lung surgery [34]. Because of the ability to precurve very small elastic tubes, manipulators of this type are able to work in very small spaces. We investigate the possibility of an independently controlled concentric-tube manipulator for endoscopic deployment, and Figure 2.2 depicts our initial system design.

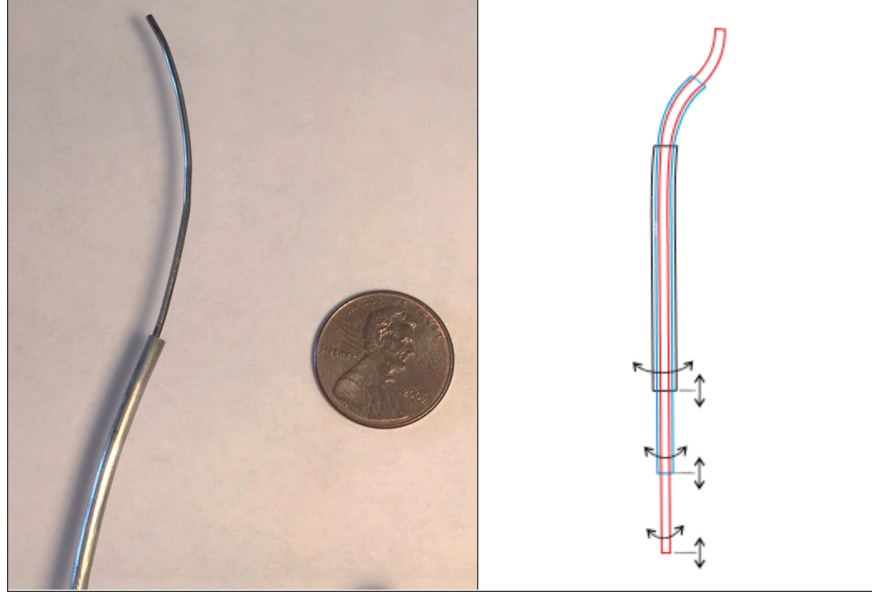


Figure 2.1: Concentric tube manipulators can be manufactured to needle sizes, as shown on the left. Many degrees of freedom are achieved by grasping the base of each tube and both translating in the axial direction and rotating about the centerline axis.

2.1.1 Overlap Constraint

In prior analysis of concentric tube kinematics, most pre-curved tubes have been designed with a single section of curvature at the distal end of the tube. For these types of designs, curved sections on separate tubes frequently overlap, causing an increase in internal moments and creating torsion. Therefore, we constrain the design space to avoid the overlap of curved sections altogether and thereby eliminate the potential for torsional instability [6, 26]. We hypothesize that designs of this type are advantageous for robots which require a long, winding transmission path, as is the case in endoscopic procedures.

In our proposed class of designs, we let all *outer* tube designs contain *straight* sections at their distal ends, with lengths that are greater than or equal to the length of the sum of all curved section lengths on *smaller* tubes. Then, tubes with pre-curvature contain segments which follow the order: straight \rightarrow curved \rightarrow straight. This is in contrast to most prior designs, which have simply been straight-curved. We define L_{s_i} and L_{c_i} as the lengths of the straight and curved distal sections of the i^{th} tube, beginning from the base. Then, assuming there are at most two straight sections and one curved section in each tube design, the new

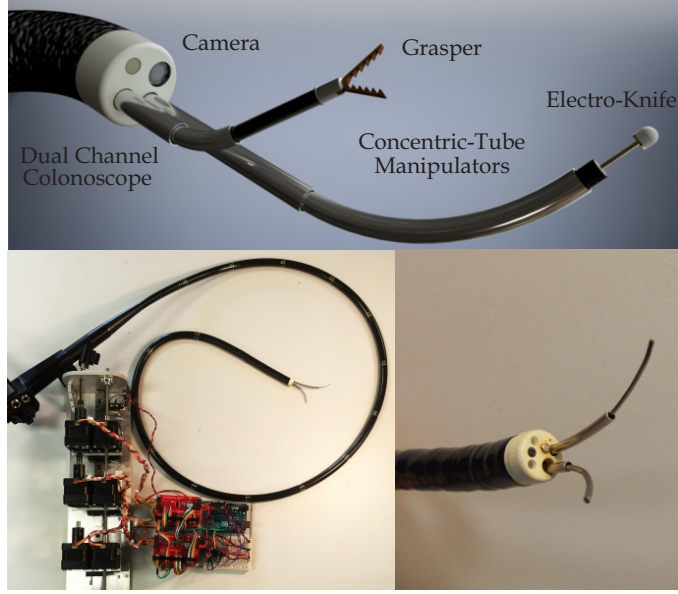


Figure 2.2: Initial system design.

section length constraint can be described as

$$L_{s_i} \geq \sum_{k=1}^{i-1} L_{c_k}. \quad (2.1)$$

Overlap of curved sections is then only possible when an inner tube is withdrawn far enough that its tip is further retracted than the tip of the next outer tube. This type of actuation does not result in any useful configurations, and therefore is disallowed in any control scheme.

2.2 CTR Modeling

In order to meet the design specifications, we modeled the kinematics of a collection of nested concentric tubes. The modeling is based on the work done by Rucker et al., which applied geometrically exact Kirchhoff rod theory to pre-curved concentric tubes under arbitrary external point and distributed wrench loading [25]. Friction is neglected in this modeling framework, but as discussed in Ref. 25, its effects do not appear to dominate prototype behavior.

Table 2.1: Table of concentric tube kinematics variables.

Variable	Definition
g_1	Transformation describing the deformed backbone shape of the collection of tubes
$u_{i,j}$	Curvature of the i^{th} tube about the local j axis, where the innermost tube is $i = 1$
θ_i	Angular rotation of the i^{th} tube about the local z-axis with respect to the 1^{st} tube
\mathbf{e}_3	Unit vector on local z-axis ($[0 \ 0 \ 1]^T$)
R_1	Rotation matrix for the first tube relative to global reference frame
R_{θ_i}	Rotation matrix (about the z-axis) for the i^{th} tube relative to the 1^{st} tube by the angular amount θ_i
\mathbf{f}	Distributed applied load
\mathbf{l}	Distributed applied moment
K	Stiffness matrix
E	Young's modulus
I	Second moment of area of tube cross section
G	Shear modulus
J	Polar moment of inertia of tube cross section

2.2.1 Kinematics Overview

The derivation of the model below is described in Ref. 25. The resulting multi-tube kinematics and statics are defined by a set of first order differential equations for the set $\{g_1, \mathbf{u}_1, u_{2,z}, \dots, u_{n,z}, \theta_2, \dots, \theta_n\}$, as follows:

$$\dot{g}_1 = g_1 \hat{\boldsymbol{\xi}}, \quad \text{where } \boldsymbol{\xi} = \begin{bmatrix} \mathbf{e}_3^T & \mathbf{u}_1^T \end{bmatrix}^T \quad (2.2)$$

$$\begin{aligned} \begin{bmatrix} \dot{u}_{1,x} \\ \dot{u}_{1,y} \end{bmatrix} &= -K^{-1} \sum_{i=1}^n \left(R_{\theta_i} \left(K_i \left(\dot{\theta}_i \frac{dR_{\theta_i}^T}{d\theta_i} \mathbf{u}_1 - \dot{\mathbf{u}}_i^* \right) + (\hat{\mathbf{u}}_i K_i + \dot{K}_i)(\mathbf{u}_i - \mathbf{u}_i^*) \right) \right) \Big|_{x,y} \\ &\quad - K^{-1} \left(\hat{\mathbf{e}}_3 R_1^T \int_s^\ell \mathbf{f}(\sigma) d\sigma + R_1^T \mathbf{l} \right) \Big|_{x,y} \end{aligned} \quad (2.3)$$

$$\dot{u}_{i,z} = \dot{u}_{i,z}^* + \frac{E_i I_i}{G_i J_i} (u_{i,x} u_{i,y}^* - u_{i,y} u_{i,x}^*) + \frac{(\dot{G}_i J_i)}{G_i J_i} (u_{i,z}^* - u_{i,z}) - \frac{1}{G_i J_i} \mathbf{e}_3^T R_i^T \mathbf{l}_i \quad (2.4)$$

$$\dot{\theta}_i = u_{i,z} - u_{1,z}. \quad (2.5)$$

Variable definitions are listed in Table 2.1. Each variable can be expressed as a function of arc length s , and all dots denote a derivative with respect to s . The $*$ superscript refers to the variable *before* it undergoes deformation in the nested state, which means solutions require tube pre-curvatures that are some known functions of arc-length. The $\hat{}$ operator refers to a conversion of an element of \mathbb{R}^3 to its corresponding element in $\mathfrak{so}(3)$, as defined in Ref. 19. The x and y curvature components of the outer tubes are not necessary for describing the shape of the manipulator because in a collection of nested concentric tubes, the deformed curves of all tubes follow the same trajectory. The main distinction from a single rod is that the tubes are free to twist independently about the local tangent z-axis.

The entire system is constrained by actuator inputs (rotations and translations) at the proximal end and static equilibrium conditions at the distal end. To implement the forward kinematics, we solve the resulting boundary value problem by numerically integrating the first order system described in Equations 2.2 - 2.5 for a given set of actuator inputs and guessed initial curvatures at the entry point of the manipulator. A shooting method is then

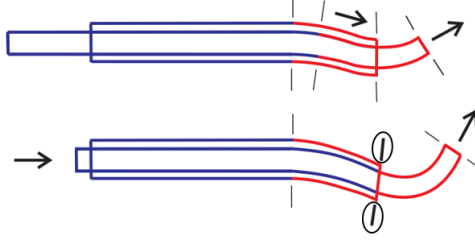


Figure 2.3: At overlap of deformed curvature step transitions, the manipulator Jacobian is discontinuous. Relative translation of the tubes at across this overlap point causes an instantaneous change in direction of end effector velocity.

used to iteratively find the initial curvatures that satisfy the static equilibrium at the distal end.

2.2.2 Jacobian Discontinuities

Traditionally, concentric-tube robots are designed with discrete sections of pre-curvature and abrupt transitions between sections in order to maximize dexterity. Consequentially, the axial sliding motion of one tube with respect to another will result in discontinuous end-effector motion at certain points in the workspace. In Figure 2.3, an example concentric-tube design is shown in a configuration where two sources of deformed curvature discontinuity overlap. Sections of initially straight tube are colored blue, and pre-curved sections of tube are colored in red. Specifically, the end of the outer tube occurs at the exact same arc-length location as the step change in pre-curvature of the inner tube. At this configuration, the manipulator Jacobian is discontinuous. As a demonstration of this behavior, Figure 2.4 shows a series of plotted manipulator poses corresponding to a similar concentric-tube design to what is shown in Figure 2.3. The plotted poses are simulated by solving the forward kinematics model using the method described in Section 2.2, where the inner tube is translated in the distal direction by increments of 0.1 mm . In this simulation, the abrupt change in motion direction occurs when the point of inner tube pre-curvature transition aligns with the tip of the outer tube. This event happens halfway through the translation of the inner tube. This discontinuous motion can be a source of error for inverse kinematics

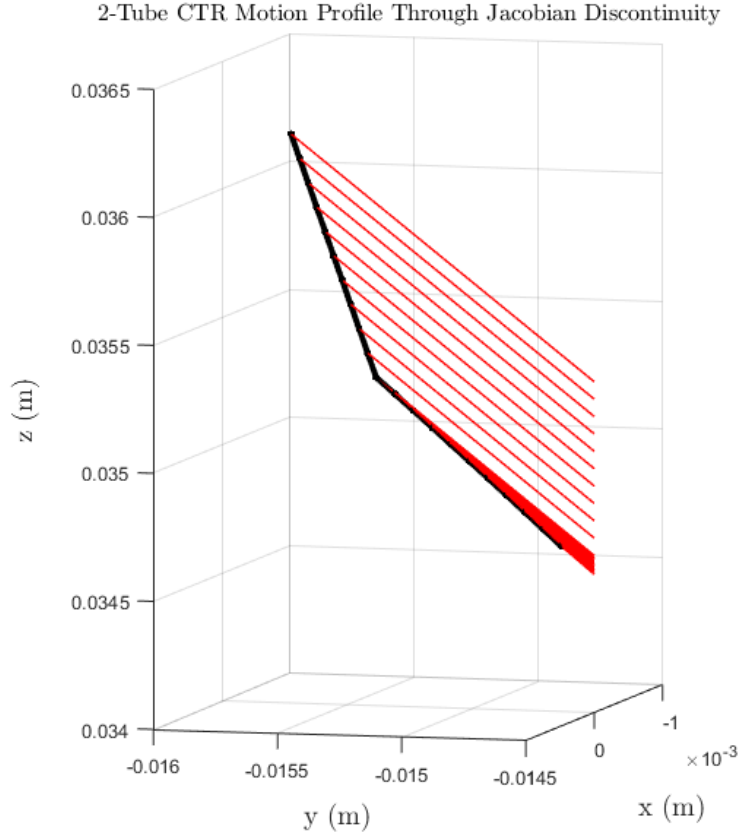


Figure 2.4: Multiple manipulator shapes are simulated as the actuators sweep through a problematic configuration, and the plot is focused on the distal ends in order to highlight tip position. Red lines represent the distal end of the manipulator, and the black line connects all of the end effector positions to represent the motion profile. As the tubes are actuated through an overlap of parameter discontinuities, the motion of the manipulator end effector encounters an abrupt change in direction.

approaches that use a finite difference approximation of the Jacobian. When a desired motion must converge to or pass through points of Jacobian discontinuity, these methods may produce erratic end effector motion if the target error becomes less than the finite difference step. This can be easily avoided by choosing a step size that is appropriately small. Alternatively, it may be desirable to model smooth pre-curvature transitions since it not only precludes any discontinuities, but also can more accurately model tube geometry. In a recent study, Ha et al. designed concentric tubes with piecewise straight sections in order to avoid pre-curvature overlap and reduce elastic instability [10]. Their model used sigmoid functions to approximate pre-curvature transitions because their manufactured tubes did not achieve a truly instantaneous step change as modeled. These sigmoid curves can be plotted with logistic functions with the general form

$$f(x) = \frac{L}{1 + e^{-k(x-x_0)}}, \quad (2.6)$$

where L is the magnitude of the step change, x_0 is the location of the transition midpoint, and k is the steepness of the transition curve. A linear combination of multiple logistic functions can be used to approximate tube designs with multiple discontinuous changes in pre-curvature. Ideally, the functional approximations will mimic the physical tube curvature exactly. This greatly depends upon the choice of steepness factor k , where large magnitudes of k will cause transitions to occur almost instantaneously over very small arc-length travel. This modeling approach also allows kinematics models to solve the system of differential equations (2.2 - 2.5) in a single integration, without subdividing the manipulator length. This means that choices of k for all pre-curvature functions are limited by the ability of numerical techniques to integrate over smooth, fast changes that closely resemble discontinuous changes. Decreasing the integration step size will enable many numerical solvers to handle this issue, but it comes at the cost of computational efficiency.

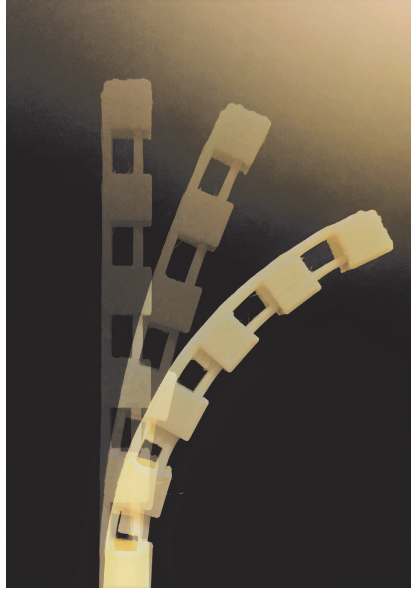


Figure 2.5: The CAAR accomplishes planar bending through relative translation of the tube bases. Movement of the offset backbones causes a moment at the distal end, resulting in bending. The design shown here consists of uniform cut geometry, resulting in a bending shape of constant curvature.

2.3 Concentric Agonist-Antagonist Robots

The concentric agonist-antagonist robot (CAAR) is a recently proposed continuum robot design that uses push-pull actuation to achieve bending in a plane [20]. It consists of concentric, elastic tubes which are fixed together at the distal end and not free to slide relative to one another as in the case of concentric-tube robots. To create conditions for bending, material is selectively removed from each tube such that the neutral bending axis is offset from the centerline (see Figure 2.5). When the tube bases are translated in opposite directions, the forces induced by the offset backbones generate a moment at the manipulator tip, and bending occurs. This design is similar to the wrist developed by York et al, which actuated a notched elastic tube by pulling a tendon [30, 37]. However, the CAAR uses push-pull motion of two backbones to bend within a full plane instead of a half-plane. A key advantage in this design is that bending can be achieved through a large range of angles without experiencing any of the elastic instabilities observed in many concentric-tube manipulators. In particular, the CAAR can pass through the completely

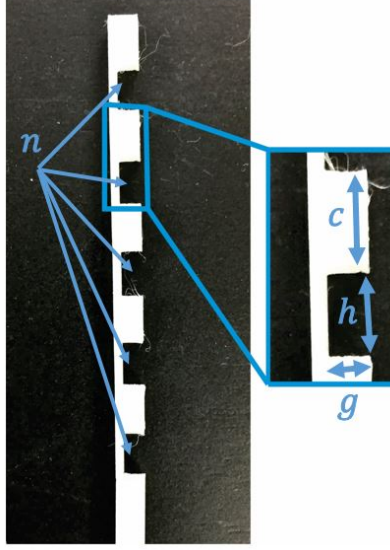


Figure 2.6: The four basic geometrical parameters shown here determine the shape of the CAAR during actuation.

vertical configuration with ease, whereas this motion is impossible for many highly pre-curved concentric-tube robots. By tuning the geometry design for material removal, the CAAR is able to curl into high-curvature shapes within small regions such as the colon workspace. In the following section, we introduce the kinematic equations that relate the tube base translations to end effector displacement. We use this framework to design a manipulator that can be endoscopically deployed.

2.4 CAAR Modeling

As shown in Figure 2.6, the basic shape of the CAAR is parameterized by four design features, assuming no pre-curvature exists in either tube: (1) cut depth g , (2) cut section height h , (3) uncut section height c , and (4) number of cut segments n . In Ref. 20, Oliver-Butler et. al characterized the effects of varying the cut section height and orientation about the centerline axis. In our endoscopic design case, we choose to simplify the design space by using uniform cut geometry. In this constrained parameter set, the manipulator will always bend into circular arcs of constant curvature. For these uniformly bending CAAR

manipulators, the planar shape is fully determined by the total arc length s_L and the angle of the end effector from the horizontal. The angle can be easily computed using the distance between the centroids of each cut tube ($\bar{y}_1 + \bar{y}_2$) and the relative translation of the two tubes ($\Delta \mathbf{q}$):

$$\theta = \frac{\Delta \mathbf{q}}{\bar{y}_1 + \bar{y}_2}. \quad (2.7)$$

Depending on cut geometry, the centroids of each tube may require careful computation. For a detailed explanation of an example neutral axis calculation, see Ref [20](#). Once the end effector angle is found, the total arc length along the manipulator centerline is simply the sum of each section length:

$$s_L = (nh - \bar{y}\theta) + c(n - 1) + b. \quad (2.8)$$

where \bar{y} is the neutral axis of the larger tube and b is any length beyond the last cut section. Given both θ and s_L , it is simple to build a base-to-tip transformation in the x-z plane, based on work done by Webster et al in Ref. [35](#):

$$T_{bend} = \begin{bmatrix} \cos \theta & 0 & \sin \theta & \frac{s_L(1-\cos \theta)}{\theta} \\ 0 & 1 & 0 & 0 \\ -\sin \theta & 0 & \cos \theta & \frac{s_L \sin \theta}{\theta} + q_2 \\ 0 & 0 & 0 & 1 \end{bmatrix}. \quad (2.9)$$

It is desirable to also rotate the tubes axially in order to sweep the planar range of the manipulator through 3-dimensional space. We can easily define a rotation angle ψ that describes the tube base rotation about the z-axis. Then, the updated end effector transformation can be found by simply pre-multiplying Equation [2.9](#) by

$$T_{rot} = \begin{bmatrix} \cos \psi & -\sin \psi & 0 & 0 \\ \sin \psi & \cos \psi & 0 & 0 \\ 0 & 0 & 1 & 0 \\ 0 & 0 & 0 & 1 \end{bmatrix}, \quad (2.10)$$

which completes the necessary set of equations for computing the forward kinematics.

2.5 Manipulator Simulation Analysis

2.5.1 CTR Workspace

We began our workspace simulations by defining the basic structure of each manipulator. The CTR is composed of 3 nested concentric tubes that follow the curvature guidelines specified in Section 2.1.1. We determined the reachable workspace of the manipulator by uniformly sampling the actuation space with a resolution of 2 mm in translation and 30 degrees in rotation. At each sampled point, the forward kinematics was solved within the user defined tolerance. The point cloud in Figure 2.7 represents the set of Cartesian coordinates that the robot could reach. This set was generated using the design parameters found in Table 2.2. The large values of proximal straight section lengths are required for full travel through a standard colonoscope, and this parameter does not affect the workspace of the manipulator. For context, we simulated the bounds of the colon (in pink), and the 140 degree field of view of the colonoscopic camera (in brown). An iterative simulation process was performed in order to characterize the effect of the other design parameters. Early in the design process we discovered that in a 3-tube assembly, any pre-curvature in the outermost tube greatly reduced the reachable workspace within the colon wall. This is because the overlap constraint has an accumulating effect on the length of distal straight sections for outer tubes, and this reveals a trade-off introduced by the overlap constraint. We therefore limited 3-tube designs

Table 2.2: CTR manipulator design parameters for workspace simulation.

Tube	OD (mm)	ID (mm)	Pre-Curvature (m^{-1})	Proximal Straight Length (mm)	Pre-Curved Length (mm)	Distal Straight Length (mm)
Inner	2.54	2.25	40	1574	20	0
Middle	2.87	2.57	35	1624	25	20
Outer	3.43	2.92	0	1674	0	45

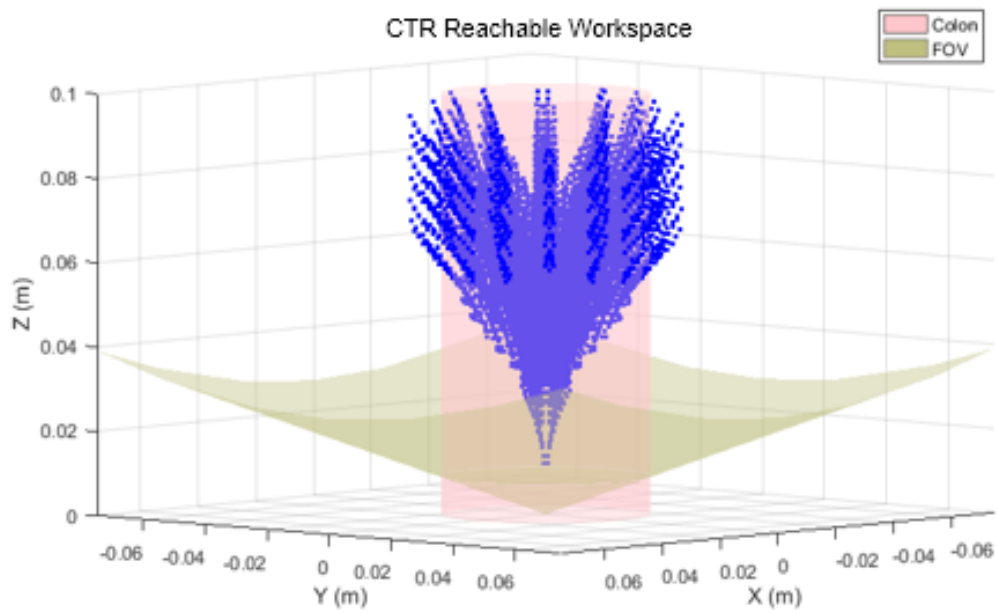


Figure 2.7: The workspace of the concentric tube manipulator with an overlay of the colon in pink and the field of view of the colonoscope in gray. A hole in the center of the workspace grows as the manipulator is inserted further into the colon.

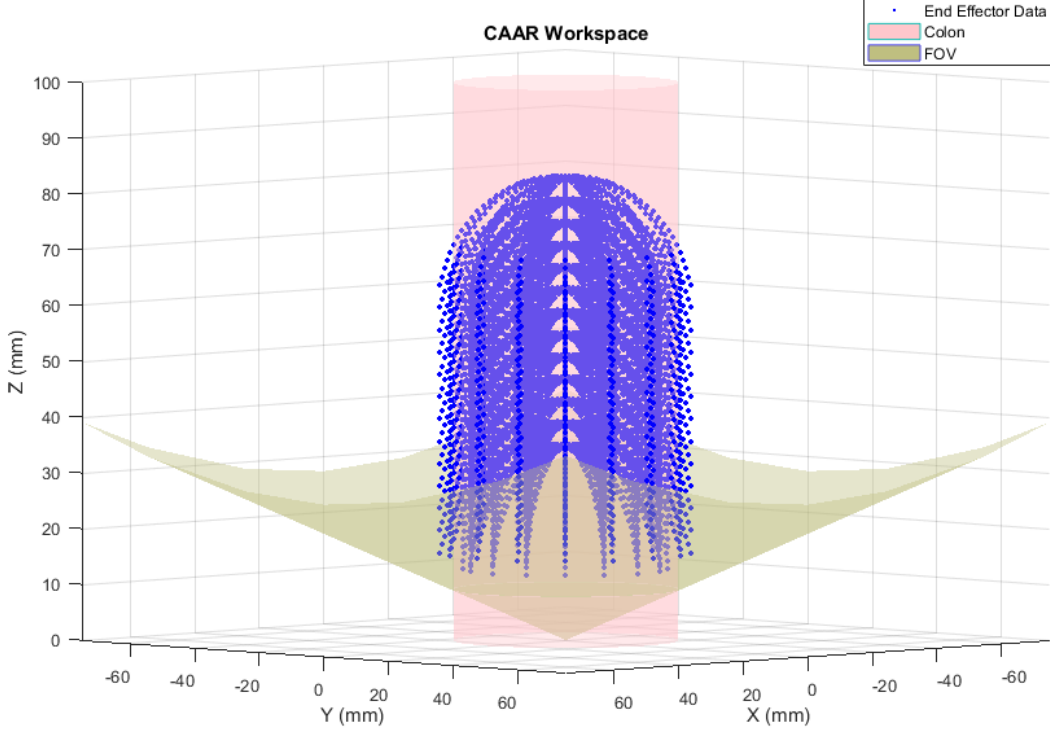


Figure 2.8: The workspace of the CAAR with an overlay of the colon in pink and the field of view of the colonoscope in gray. Unlike the CTR, the CAAR has a uniform reach in the xy-plane regardless of insertion depth.

to have straight outer tubes. Then, increasing pre-curvature and pre-curved lengths of the middle and inner tubes yielded workspaces with increasingly better coverage but diminishing spatial resolution. We observed that all CTR workspace simulations exhibited a changing xy-plane dexterity as the manipulator was inserted further into the colon along the z-axis. At relatively high z-coordinates, the CTR contains a large cone-shaped hole in the center of its workspace in which it cannot maneuver.

2.5.2 CAAR Workspace

To simulate the CAAR workspace, we performed a forward kinematics loop similar to the one described in the previous subsection. The example manipulator consists of two tubes with cut geometry listed in Table 2.3. The workspace was generated by iterating each tube base translation by 2 mm and rotating both tubes simultaneously by 30 degrees. At each

Table 2.3: CAAR manipulator design parameters for workspace simulation.

Tube	OD (mm)	ID (mm)	n	c(mm)	h(mm)	g(mm)	b(mm)
Inner	2.0	1.1	6	2.9	2.9	0.5	2.9
Outer	3.2	2.4	6	2.9	2.9	0.4	2.9

configuration, we used the transformations described in Equations 2.9 and 2.8 to compute the end effector position and plotted all the data on the spatial plot shown in Figure 2.8. Because of the constant curvature design, the CAAR workspace is evenly distributed inside a cylindrical shape. The depth of insertion into the colon does not change the xy-plane dexterity, which is an advantage in comparison to the CTR workspace. Changing the cut and uncut section lengths h and c can expand or shrink the workspace volume, and the cut depth g affects the degree of constant curvature bending. Additionally, the orientation of the end effector at the simulated colon wall is advantageous for performing tasks there.

2.5.3 Resolution Analysis

We measured positional accuracy of both types of robots by limiting joint resolution according to the selected stepper motors for the actuation system (see Chapter 4). We modeled this limitation by computing the resolution of the instrument tip using the minimum step angle specification of 1.8° for each motor, which converts to 0.025 mm of translation through the lead screw. More precision is possible through microstepping, but for preliminary analysis, we consider motor control to be without this capability. The computation for the resolution shown in Figure 2.9 was performed for the same designs analyzed in Section 2.5.1. In order to show end effector spatial resolution across the workspace, we sampled the actuation space to find an initial set of >3000 nominal manipulator configurations. For each point in this group, an *additional* subset of points was solved corresponding to a minimum step by each actuator away from the nominal point. Then, we calculated the maximum Euclidean distance that the end effector could travel away from the nominal configuration by referencing the subspace bounded by the new subset. This maximum Euclidean distance

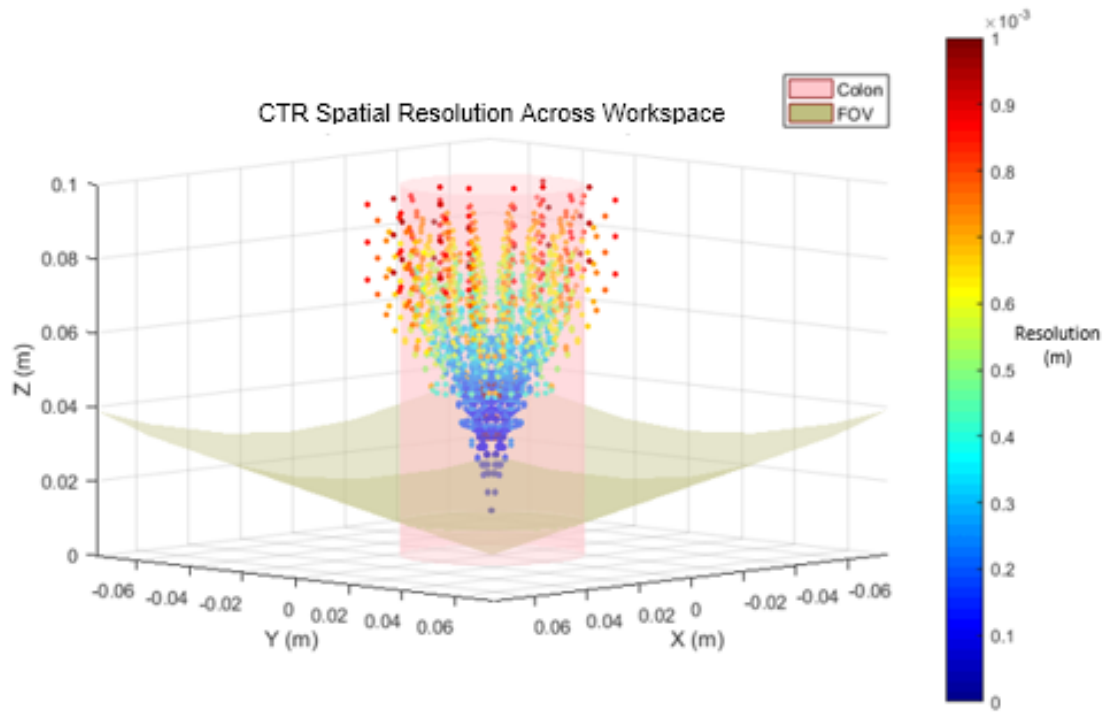


Figure 2.9: The spatial resolution of the CTR end effector is represented as the color of each point in the workspace.

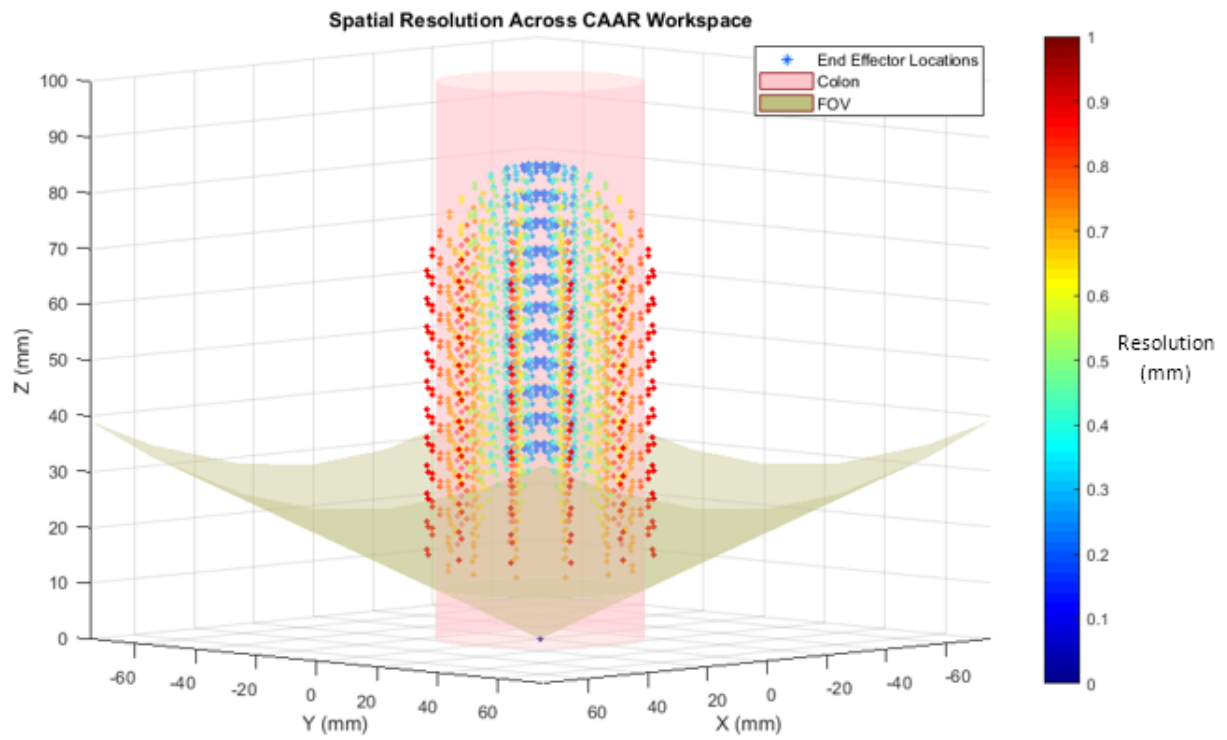


Figure 2.10: The spatial resolution of the CAAR end effector is represented as the color of each point in the workspace.

represents a measure of spatial resolution in that it defines an upper bound on the end effector displacement that is caused by minimum actuator steps. Figures 2.9 and 2.10 show a workspace point cloud for each type of robot, in which the color scale represents the spatial resolution.

2.6 Discussion

Based on the results of the workspace and resolution analyses we performed, it is possible to design a set of CTR and CAAR manipulators that fulfill the design requirements introduced in Chapter 1. However, the CTR design required highly pre-curved sections of tubing to access a comparable workspace to the CAAR, which may cause instability problems. In addition, the CAAR has better access to the center of the colon than the CTR and an overall more uniform workspace. Both manipulators have enough end effector spatial resolution to navigate the colon, even if driven by an inexpensive stepper motor actuation system. It is possible to improve the resolution by replacing the actuation system, but it likely comes with much higher motor prices.

The following chapter discusses the design of the transmission tubes which lie inside the colonoscope and connect the distal manipulator to the motors. The manipulator design analysis we have discussed so far assumes that the motor translation and rotation can be perfectly transmitted to the end of the colonoscope. This is not necessarily the case, and solving this issue poses a primary engineering challenge for this system.

Chapter 3

Transmission Design

In order to deploy a continuum robot out of the end of a standard colonoscope, the instrument structure must have sufficient length to travel more than 7 feet through a tool channel (see Figure 2.2). Our initial design of the surgical system assumed that the section of the manipulator that lies entirely inside the colonoscope could be made of any available tubing material that met the size restrictions of the tool channels. However, early investigation of interaction between commonly-used tubing for continuum robots and the colonoscope revealed that the transmission tubes must be significantly more flexible than previously thought. We desire that the natural flexural rigidity of the colonoscope should not be greatly increased by the addition of the manipulator.

Also, as shown in Figure 3.1, the entry port for the tools contains an abrupt angle of approach, which only allows tubes with higher strain limits to pass through. This further restricts the range of shafts that will physically pass through the tool channels of the colonoscope. The following sections explain the process by which we approximated the flexural rigidity of the colonoscope and our proposed solutions for transmission design.



Figure 3.1: The tool entry at the proximal end of the colonoscope contains a sharp angle to pass through.



Figure 3.2: Colonoscope flexural rigidity experiment.

Table 3.1: Colonoscope bending test data.

L (<i>m</i>)	Applied Force (<i>kg</i>)	Deflection (<i>m</i>)	EI (<i>Nm</i> ²)
0.1	0.25	0.003	0.0307
0.1	0.40	0.040	0.0274
0.1	0.56	0.050	0.0272
0.2	0.08	0.067	0.0276
0.2	0.14	0.107	0.0238
0.2	0.25	0.140	0.0211
0.2	0.30	0.150	0.0196
0.3	0.08	0.165	0.0271
0.3	0.13	0.197	0.0307
0.3	0.19	0.227	0.0256

3.1 Colonoscope Constraints

3.1.1 Colonoscope Bending Test

In order to define a maximum permissible flexural rigidity for the robot transmission section, a simple experiment was performed to approximate the flexural rigidity of the colonoscope. The experimental setup is shown in Figure 3.2. We used the same rod model introduced in Section 2.2 to describe the shape of a section of the colonoscope as a cantilevered elastic rod, where we assumed that the colonoscope exhibits linear elastic deformation under load excluding the actuated distal section. Using a spring scale with a digital read-out, we applied a load in the x direction to the end of the bending section of the colonoscope. The opposite end of this section was fixed using a clamp. Since the experiment was performed on a flat surface, the effect of gravity is negligible. By measuring the deflection of the colonoscope at the location of the load, we can solve the boundary value problem of static equilibrium by guessing the flexural rigidity EI of the colonoscope along with the values of the unknown state variables at the cantilevered end. The results of this experiment are shown in Table 3.1. Three segments of different length were tested using varying applied forces. The values of EI vary in the range of $0.02 - 0.03 \text{ Nm}^2$, with the average being 0.0261 Nm^2 . The inconsistency in these values can be attributed to unknown elastic behavior of the colonoscope, as it is not composed of uniform material. We use these results to establish an approximate specification

Table 3.2: Transmission design requirements.

Requirement	Value
Flexural Rigidity (Nm^2)	≤ 0.026
Max. Elongation (mm)	≤ 5
Max. Windup (deg)	≤ 90

for the stiffness of endoscopic robot transmissions. As an example comparison, the combined flexural rigidity of three Nitinol tubes in parallel that fit inside the colonoscope tool channels equals $0.3125 Nm^2$, which is much higher than desired. This result indicates that the manipulator will require a significantly more compliant transmission section than previously thought in order to decrease the overall flexural rigidity that is added to the colonoscope.

3.1.2 Transmission Requirements

Using the results of the colonoscope bending test and observations of alternative tubing options, we developed a set of desired requirements for the transmission tubing. These are listed in table 3.2. The maximum elongation and rotational windup values do not necessarily correspond to an error metric for the manipulator, but we hypothesize that transmission designs which meet the requirements will function well enough for compensation in the control approach. For example, the 5 mm elongation requirement ensures that the bending motion of the manipulator does not lag significantly behind the relative translation of the tubes due to elastic axial stretching, and can be adjusted for in real-time. All of the tubes selected for further study in the following sections meet the flexural rigidity requirement.

3.2 Candidate Transmission Designs

3.2.1 Notched Transmission Approach

In our initial manipulator design, we planned to create an instrument made entirely of Nitinol because this material has proven ideal for many concentric-tube studies. However, since we discovered that Nitinol tubes with appropriate diameters would greatly increase the flexural

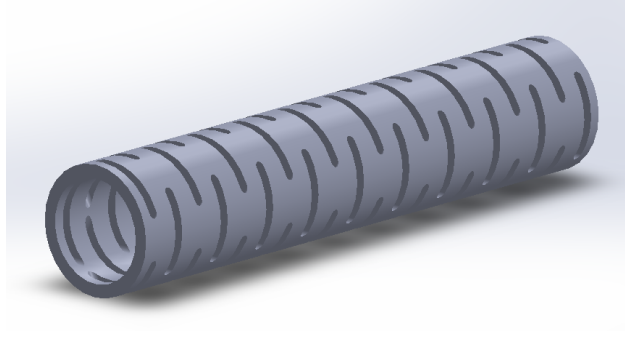


Figure 3.3: A solid model of a stainless steel notched tube design for the robot transmission, based on the work done Lee et. al[16].

rigidity of the colonoscope, we proposed a machined metal tubing alternative. We modeled a manipulator with a transmission made of structurally modified stainless steel tubes, which are joined to Nitinol sections at the distal end. The stainless steel tubes have a Young's Modulus of around 200 GPa (an increase by a factor of 3 from the Nitinol tubes). In order to decrease the flexural rigidity, these tubes were designed with notched arranged in a pattern similar to the one studied in Ref. 16. Figure 3.3 depicts a solid model of a representative notched tube, for which we determined stiffness values by applying finite element analysis to designs of this type under defined loading. This particular design was shown to decrease flexural rigidity while maintaining a relatively high torsional stiffness. The notches were designed so that the flexural rigidity of the colonoscope was only increased by 50% due to the stainless steel transmission tubes.

However, for the notched patterns that achieved the desired flexibility, the spacing and notch width dimensions were in sub-millimeter ranges. This requires highly precise and time-consuming machining of thin-walled tubes, which is beyond the capability of the available university facilities. We obtained quotes from laser cutting manufacturers that exceeded the budget of this project. In addition, one of the goals of the overall system design is to provide an affordable, modular benchtop system. We therefore continue our study with alternative transmission designs and leave investigation of structurally modified transmissions to future work.



Figure 3.4: 3D-printed transmission composed of 10-inch long segments joined together. The inner lumen allows passage of a cable for grasping actuation of a surgical instrument.

3.2.2 FDM Printed Tube

We also investigated the transmission capabilities of available 3D printing materials using fused deposition modeling (FDM). There are several materials that have been recently produced that have excellent flexural properties and strain limits. We found that the Eastman Amphora™ 3D Polymer HT5300 is optimal for slender, flexible structures. It has a flexural modulus of 1575 MPa and a 7% strain limit; this makes for tubes with high amounts of recoverable bending and sufficient axial stiffness. Figure 3.4 contains a tube printed with HT5300 that can be inserted through the entire colonoscope. Since the length of this tube must be approximately 2000 *mm* to reach the distal end, we could not print the entire length on available printers. Instead, we printed 10 inch segments that were joined together with Loctite and small joint tubing pieces. The resulting structure is a highly flexible tube with an inner lumen that allows a cable for surgical graspers to pass through.

3.2.3 Purchased Tubes

As shown in Figure 3.5, we considered several commercial tubing options for the transmission design, including plastics such as PEEK (polyetheretherketone) and Nylon, as well as carbon fiber and a sample of helically-wrapped metal strand tubing obtained from Fort Wayne Metals. In addition, we considered designs of the CAAR robot which used a surgical grasper

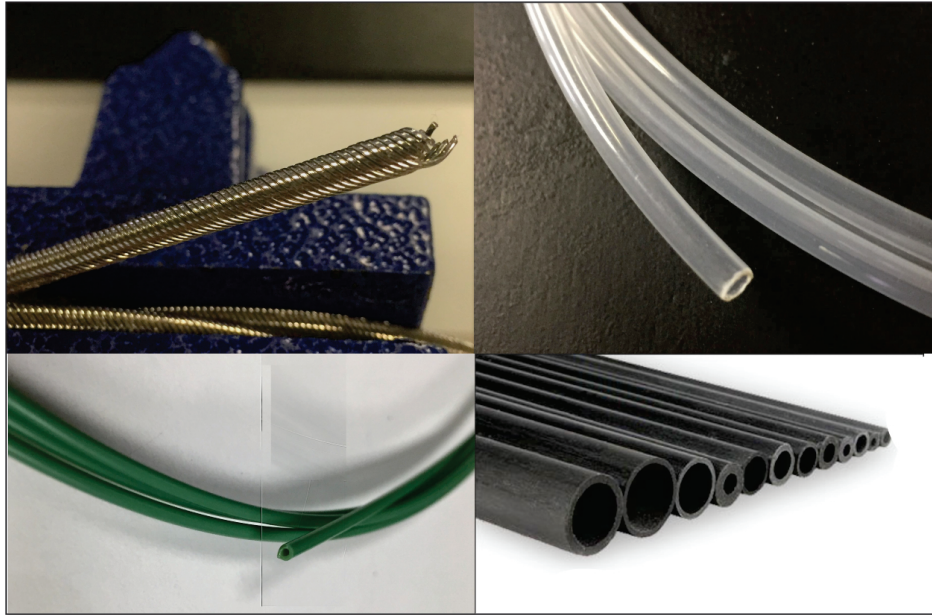


Figure 3.5: Several off-the-shelf tubing options were considered for transmission design. **(Top Left)** Helical Hollow Stranded tubing is composed of helically wrapped strands of steel or Nitinol and is well-suited for transmitting torsion through curved paths (credit FW Metals). **(Top Right)** Nylon tubing provides high axial stiffness and a lubricious surface for sliding against inner tubes. **(Bottom Left)** PEEK plastic tubing is an alternative to steel tubing and is available in very small sizes. **(Bottom Right)** Carbon fiber tubes are available in large straight lengths, and small diameter sizes have enough flexibility to integrate into the colonoscope.

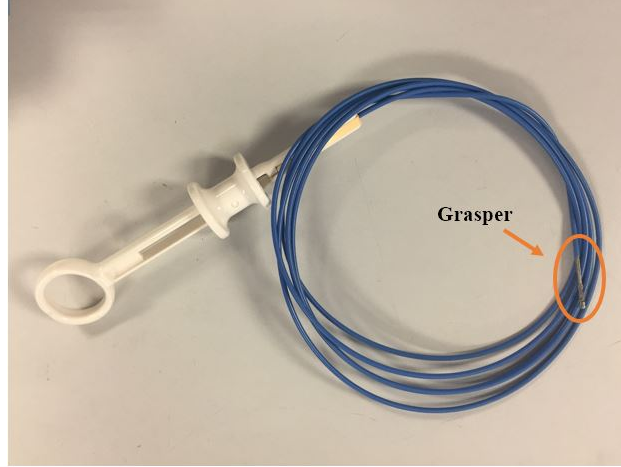


Figure 3.6: We acquired several surgical graspers for teleoperation experiments and investigated the use of the grasper shaft as the inner transmission.

in place of the inner tube. Bending motion can be achieved with an uncut inner tube, the tradeoff being a smaller moment arm which leads to higher actuation forces. Figure 3.6 shows an example of a grasper typically used in endoscopic procedures.

The variety of materials and shaft structures provides many potential combinations of transmission tubing to actuate the robot. In the next section, we list the tested combinations and assess the their ability to drive the tube motion.

Table 3.3: Transmission design results under full actuation range for both straight and looped transmission paths.

Material	Type	Straight		Curved	
		Elongation (mm)	Windup (deg)	Elongation (mm)	Windup (deg)
Nylon	Outer	4	45	10	No distal rotation
HT5300	Inner	<1	10	5	>360
HHS	Outer	8	<1	19	3
HHS	Inner	22	0	30	10
PEEK	Inner	<1	10	3	270
Carbon Fiber	Inner	0	0	0	0 (choppy)
Surgical Grasper	Inner	7	22	3	95

3.3 Performance

The available sizes of the purchased tubes as well as the time cost of manufacturing the 3D printed tubes restricted the possible combinations for testing. We completed a single 3D printed tube with an outer diameter of 2.2 mm and an inner diameter of 1 mm. This tube always functioned as the inner tube in any transmission design combination. Similarly, the only available sizes of PEEK and carbon fiber that met the flexibility requirement had small outer diameters and were only suitable for the inner tube. We found appropriate sizes of Nylon and HHS tubes that allowed them to function as outer tubes. All of the tube combinations that are listed here passed the flexural rigidity requirement by inserting them into the colonoscope and testing the ability to loop the combined system. In order to ensure their functionality during realistic colonoscopic scenarios, we tested the elongation and windup of each tube for both straight and curved constrained shapes. We used a radius of curvature of approximately 30 cm. The tubes were fitted with both CTR and CAAR prototypes printed out of HT5300 and actuated such that the full range of the workspace was accessed. In Table 3.3, we recorded the maximum observed elongation and windup during this process.

As seen in Table 3.3, most of the available flexible tubes we acquired were suitable as inner tube transmissions. Of the two outer tube options, the helical hollow strand tube provided better rotation to the distal end. Several inner tube transmissions were tested, and the best options included PEEK plastic, carbon fiber, and HT5300 filament. However, the current printing methods are not able to manufacture HT5300 tubes small enough to fit inside the available outer HHS tubes. Therefore, we chose to move forward with transmission designs containing PEEK, carbon fiber, and HHS tubes. None of these options can be expected to perfectly transmit translation and rotation to the distal end, but any lag in the movement may be correctable with an intuitive controller. In the following chapter, we describe the prototype manipulator that is tested for teleoperation and discuss its positioning capability.

Chapter 4

Prototyping & Testing

4.1 Manipulator Prototyping

Many needle-sized continuum robots have been manufactured out of Nitinol (a nickel-titanium alloy) because of its superelastic properties. Our design study instead used 3D-printed tubes in order to rapidly design and test manipulators. Additionally, it was cost-effective to tune the printing process for such small sizes of manipulators. Future development of the prototypes will likely include Nitinol manufacturing, but the 3D-printed material served the purposes of this initial study.

The printed prototypes were made of the same filament described in Section [3.2.2](#), since it has excellent strain limits and flexural properties. We used both a Makerbot Replicator 2



Figure 4.1: Sample CTR prototype made of HT5300 filament.



Figure 4.2: Because of difficulty manufacturing small, thin-walled concentric tubes, alternative CAAR concepts were considered. On the left, a large channel is added to the outside of the colonoscope to accomodate a larger CAAR robot that attaches to a surgical grasper. On the right, a surgical grasper is used as the inner tube.

and a Make-it Pro M to create prototypes with layers as thin as 0.1 mm. Figure 4.1 contains an example of a printed concentric-tube manipulator, and Figure 4.2 contains early printed concepts of the CAAR manipulator integrating with a surgical tool. The final design we tested in teleoperation is shown in Figure 4.3.

4.2 Actuation System Design

We made several design choices for the actuation system to achieve compactness, modularity, and accuracy. The core of the mechanical design takes advantage of the inherent collinearity of nested concentric tubes by aligning the actuation of all joint variables on one guide rail. Hollow-shaft stepper motors serve as actuators and allow the rotation of each tube to be driven directly, without gearing, while at the same time allowing several tubes to pass through the center of its frame. We used Nanotec NEMA 17 stepper motors to drive the translation and rotation of each tube. The motors are rated for up to 25 N-cm in our desired speed range, greater than the loads necessary to actuate the robot by a factor of 10-20. This ensures the motors will not miss steps due to high load torques. We arranged the motors on a cart and guide rail system as shown in Figure 4.4. The carts and rail are THK-SSR series caged-ball linear motion guides. Each cart carries two motors: one is threaded onto

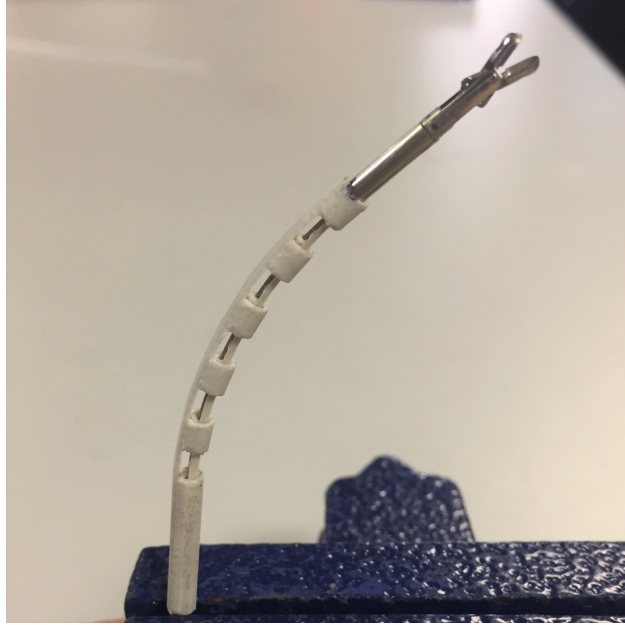


Figure 4.3: Final design of the instrument manipulator (CAAR).

a stationary lead screw to drive the linear motion of the cart, and one grips and rotates a concentric tube. Since the carriage sub-assembly can be duplicated for each concentric tube in a given design, assembly and disassembly of multiple tube designs is straightforward and time efficient. The system is easily modified for use in a variety of continuum manipulators, since many existing robot designs require prismatic and revolute joint motion aligned on a single axis.

Our stepper motors are driven by L6470 AutoDriver boards from Sparkfun. They offer an advantage in low-level access to motor commands, have relatively large electrical capacities, and are inexpensive. Each driver can be sent commands through SPI communication, reducing time and wiring complexity. The boards are controlled through the serial communication pins of an Arduino Uno. The AutoDrivers are able to receive motion commands and execute them independently while monitoring current level. Because the step counter for each motor is offset by the initial position at startup, we designed a zeroing scheme that makes use of limit switches mounted on the carriages. The switches are wired in parallel with distinct resistors and then connected to a single analog input on the Arduino.

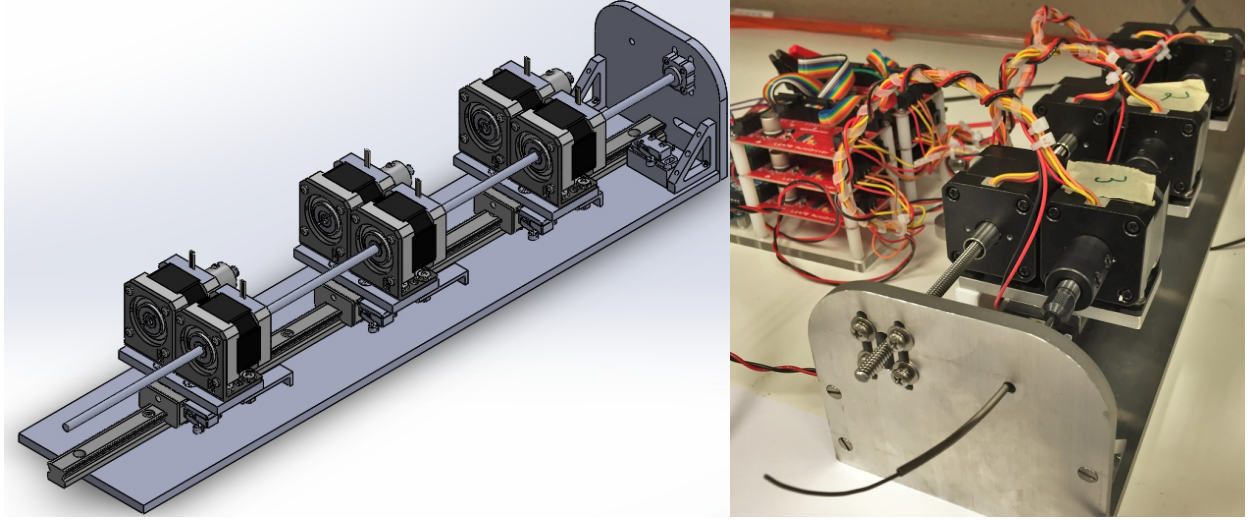


Figure 4.4: The actuation module consists of three dual motor carriages that translate and rotate the pre-curved concentric tubes while maintaining an accurate and rigid actuation platform.

4.3 CAAR vs. CTR

As discussed previously, we prototyped both concentric-tube and CAAR manipulators. During initial testing of the prototypes, it became clear that the CTR designs were less advantageous for 3-DOF endoscopic manipulation than the CAAR designs. Although the CTR designs were constrained according to the restrictions described in 2.1.1, the overlap of pre-curved tube sections with straight tube sections still generated enough axial moment to severely wind up transmission tubing during relative tube rotation and produce strong snapping to minimum energy configurations. By contrast, the CAAR does not require any relative rotation of both tubes and therefore does not induce the same kind of wind up effect.

In addition, although both types of robots are well-suited to traverse the outer wall of a cylindrical workspace such as the colon, the CTR contains a hole in the center of its workspace because of its instability in near-straight configurations. The CAAR does not have this issue and is physically able to pass through the center of the workspace. The kinematic mapping of the CAAR does contain a singularity at the exactly straight configuration. However, the inverse kinematics control approach discussed in the next section has proven successful at handling this configuration.

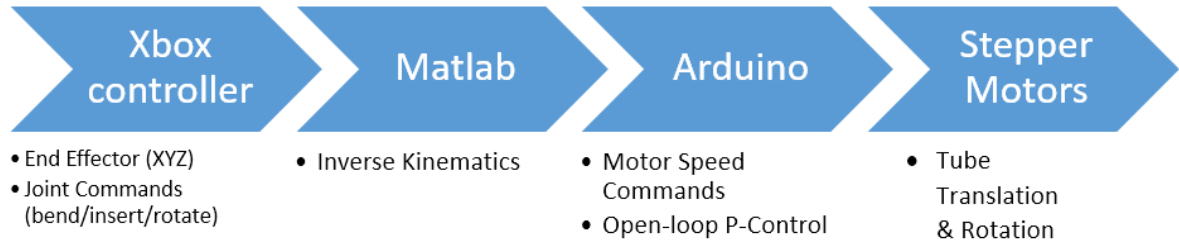


Figure 4.5: Open-loop teleoperation process from input device to actuation

4.4 Real-Time Control

We tested several basic methods of real-time position control, some more intuitive than others. All approaches were open-loop, since the stepper motors provide sufficient torque to handle tasks within the scope, and the measurement of end effector motion is qualitative in this study. The diagram in Figure 4.5 illustrates the flow of the open-loop control scheme we used to manipulate the CAAR prototype. A user manipulates the joystick and trigger buttons on a standard Xbox controller in order to intuitively move the robot in either end-effector Cartesian space or joint space. A MATLAB control scheme reads the controller data and scales it into desired robot motion. Depending upon the type of control approach being used, the MATLAB script will also solve the inverse kinematics for the joint values if necessary. The commanded joint values will be converted to motor steps and sent to the Arduino, which handles the low-level motor commands.

4.4.1 Low-Level Motion Commands

Initial testing of the stepper motor driver library revealed that the motors moved more smoothly when controlling speed instead of step angle. However, we desire to use an input device to continuously specify joint positions. In order to use the motor speed commands, we use a simple proportional control expression that gains the difference between the most recent commanded motor position and the most recently achieved motor position:

$$\dot{q}_i = K_p(q_i^{command} - q_i^{read}), \quad (4.1)$$

where K_p is a gain, $q_i^{command}$ is the commanded position, and q_i^{read} is the most recently updated position of the motor. The AutoDriver independently records and transmits the current step count while executing motion commands. Although this does not close the loop like the function of an encoder, it does provide real-time position data that is accurate to the extent that the stepper motors complete commanded steps.

4.4.2 Position Control Approaches

We developed two useful methods for solving the inverse kinematics problem in real-time. Ideally, the user would specify end effector motion in a global fixed frame and be able to view the motion for visual feedback. We can find solutions to the inverse kinematics using optimization techniques, but we found that it can be beneficial to allow the user to simply control joint space variables. This is because it becomes simpler to distinguish tube translation from rotation and overcome unexpected movement due to friction or elastic energy buildup.

Inverse Kinematics Solving

It is possible to solve for exact inverse kinematics solutions. By examining Equations 2.7, 2.9, and 2.8, we can solve for q_1 and q_2 using an optimization algorithm on the relatively simple nonlinear expressions for the x- and z-coordinates. However, the rotation angle ψ is related to the end effector position by

$$\psi = \tan \frac{y}{x}, \quad (4.2)$$

and there are two solutions for any given set of x and y coordinates. Additionally, it is not trivial to perform rotations that exceed values of $\pm 2\pi$.

Instead of finding exact joint values, we solved the inverse kinematics with a resolved rates approach that uses an approximated manipulator Jacobian. Although this method is likely less efficient than others, it is more than capable of handling real-time implementation. The approach is a damped-least squares algorithm that was first proposed by Wampler, which finds actuator motion corresponding to desired end effector motion by minimizing a

customized objective function [32]. The general form of the objective function is

$$F = \frac{1}{2} \left((J\dot{\mathbf{q}} - \dot{\boldsymbol{\xi}}_0)^T W_0 (J\dot{\mathbf{q}} - \dot{\boldsymbol{\xi}}_0) + \sum_{i=1}^m (\dot{\mathbf{q}} - \mathbf{v}_i)^T W_i (\dot{\mathbf{q}} - \mathbf{v}_i) \right), \quad (4.3)$$

where $\dot{\mathbf{q}}$ is the actuator velocity vector, $\dot{\boldsymbol{\xi}}_0$ is the desired end-effector twist vector consisting of linear and angular velocities, and J is the manipulator Jacobian. W_i are weighting matrices for prioritizing tasks, where W_0 gains the tracking accuracy. \mathbf{v}_i are vectors of desired actuator velocities that can be used for damping or avoiding undesirable configurations. By setting $\frac{\partial F}{\partial \dot{\mathbf{q}}} = 0$, we can find actuator velocities $\dot{\mathbf{q}}$ that minimize F . For our simulations, we set $\mathbf{v}_i = \mathbf{0}$ to achieve damping and let $m = 1$, which results in

$$\dot{\mathbf{q}} = (J^T W_0 J + W_1)^{-1} (J^T W_0 \dot{\boldsymbol{\xi}}_0). \quad (4.4)$$

The manipulator Jacobian is approximated using a finite difference approach, where the i^{th} column of the spatial Jacobian is computed as

$$J_i = \left[\frac{T_{new} - T_{nominal}}{\delta q_i} T_{nominal}^{-1} \right]^\vee, \quad (4.5)$$

where $T_{nominal}$ is the current end effector transformation, and T_{new} is the end effector transformation corresponding to a small change in the i^{th} joint value δq_i . The \vee operator converts the skew symmetric matrix product to a 6-D vector. A more detailed description of this notation can be found in Ref. 19.

Joint Space Control

We also allowed the user to directly control the basic actuation motions (bending, z-axis rotation, z-axis insertion) as shown in Figure 4.6. This control approach required no model calculations and simply scaled three signals from the Xbox controller to the appropriate proportions. In many robots, this approach leads to very unintuitive control because of the complicated mapping from joint space to task space. However, because the CAAR

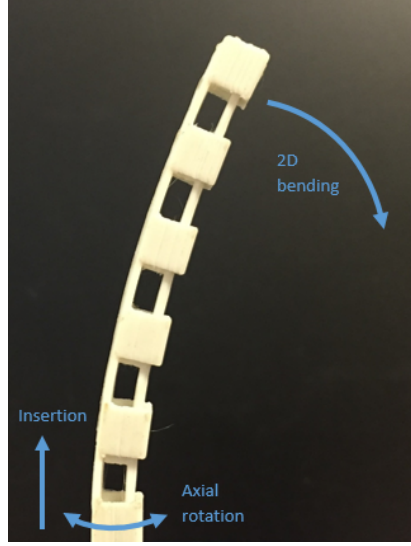


Figure 4.6: Joint space control directly maps user input to the three basic movements shown here.

manipulator has relatively simple forward kinematics, it is not overly difficult to learn control in joint space.

4.5 Results

In our first teleoperation experiment, we tested the inverse kinematics control approach by attaching the CAAR manipulator directly to the motor carriage system. This ensured that the commanded joint values were exactly at the base of the manipulator. The Xbox controller was mapped to xyz-position commands using the left joystick for motion in the xz-plane and triggers for the y-axis insertion. The basic setup is shown in Figure 4.7. In this case, the control of the end effector was easily learned for a variety of users. We performed a few trials of pick-and-place tasks in this setup, as shown in Figure 4.8. We defined a simple task of moving a hoop from one peg to an adjacent peg. All tasks were completed in around a minute.

We also performed the same pick and place tasks with the manipulator inserted through the colonoscope, using two transmission designs. Both designs used HHS tubing for the

Table 4.1: Time trial data for pick-and-place task with direct motor mounting.

Trial	Time (sec)
1	48
2	65
3	51
4	49
5	62



Figure 4.7: Position control of the manipulator end effector was intuitive with direct mounting to the actuation unit.

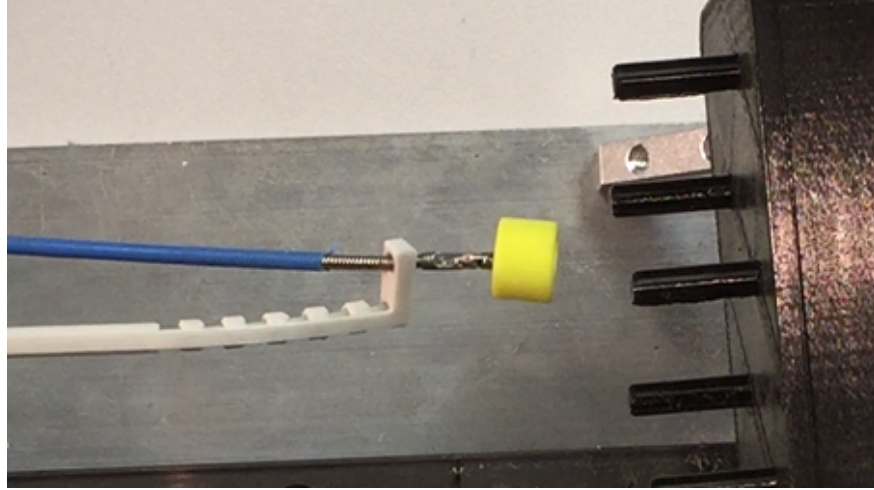


Figure 4.8: The pick and place task was performed within a minute on average when the manipulator was mounted directly on the motors.

outer tube. The inner tubes were made of PEEK and carbon fiber. It was significantly more difficult to position the end effector with the transmission through the colonoscope. In fact, the time trials could only be performed with the joint space control mapping discussed previously because the elongation in the outer HHS tube affected the bending motion enough to produce inaccuracies between the physical manipulator and the model, and the twist in both transmission tubes caused the same issue.

The data is recorded in Table 4.2. We planned to performed the trials in both straight and looped colonoscope configurations for each transmission design. However, the looped colonoscope appeared to amplify the elongation and windup effects, hindering the control of the manipulator tip. The motion of the end effector became very choppy and erratic, and it was not possible to finish the peg tasks with the rough motion.

There are many likely sources of error. During bending sequences, we observed significant axial rotation coupled to the planar bending even though no rotation was commanded. This is possibly due to unwinding of the HHS tube in tension and compression, or due to any twist in the inner tubes becoming untwisted through tension. Additionally, the transmission which used PEEK inner tubing exhibited choppy “snapping” during rotation and insertion. This is likely due to the slight precurvature of the PEEK tube, since it was manufactured in a spool. The transmission which used carbon fiber inner tubing provided smoother rotation and translation in general, resulting in improved time scores for the straight configuration.

Table 4.2: Time trial data for pick-and-place task, deployed through the colonoscope.

Trial	Time (sec)			
	PEEK		Carbon Fiber	
	Straight	Looped	Straight	Looped
1	177	-	109	-
2	195	-	85	-
3	190	-	148	-
4	205	-	82	-
5	181	-	58	-

This is likely due to the absence of pre-curvature in the carbon fiber tube. However, the carbon fiber design was not completely free of some elastic instability. The cross-sectional geometry of the carbon fiber is not manufactured in a smooth uniform circle, and this can cause jumps in rotation. Additionally, the available carbon fiber tubes had inner diameters that would not allow the standard surgical grasper cables to pass through. We instead used thin steel wire to actuate the graspers, but again the available wire is manufactured in spools with pre-curvature and likely contributed to the choppy motion experienced at the tip during the looped configuration.

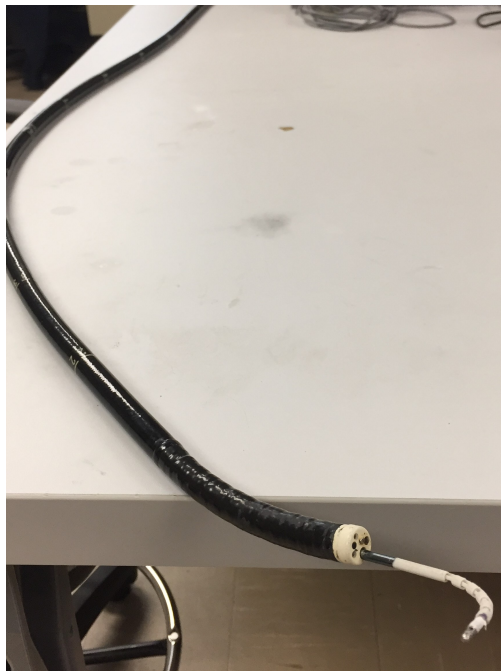


Figure 4.9: The CAAR manipulator deployed through the colonoscope.

Chapter 5

Conclusions & Future Work

We have investigated two types of concentric-tube continuum manipulators and explored their capability to function as endoscopic robotic instruments. The ability to design these types of flexible structures at needle sizes could lead to promising surgical applications such as endoscopic submucosal dissection. We have shown that in particular the CAAR will sufficiently operate within the small cylindrical workspace of the colon, and we prototyped example manipulators using FDM filament with sufficient mechanical properties.

The inherent need for axial rotation in both of these types of manipulators presents a difficult design problem. Most available tubing that sufficiently transmits torsion along a length of >7 feet is not flexible enough to adapt to the bending of the colon. Hollow Helical Stranded tube is possibly the best option for higher-diameter tubing, and it may be worth fine-tuning the stranding parameters (strand diameter, helix pitch) to optimize the axial and torsional rigidity. In smaller diameter transmissions, the lower cross-sectional moment of area allows stiffer materials to be used. However, it is difficult to access small-diameter tubing that has no precurvature, since most manufacturers stock their off-the-shelf tubes in spools. Carbon fiber may be the easiest to find readily available, but it is worth investigating the custom manufacturing of long, straight tubing in many material options.

We have also successfully implemented a simple position control approach for the CAAR robot, which demonstrated its usefulness in accessing small workspaces such as the colon. It will be worth testing the actuation system described here with a Nitinol prototype of the CAAR robot in order to evaluate the stiffness output and the required actuation forces.

Additionally, it may be worth broadening the design space to continuum robots that are actuated entirely by translation motion through the colonoscope in order to avoid the challenge of transmitting axial rotation. Future design work may include investigating the capability of flexible backbone robots with multiple planes of bending, such as the parallel continuum robot developed in Ref.'s [2](#) and [21](#). We hope the work presented here supports the development of a surgical instrument manipulator that enables better surgical care for endoscopic procedures.

Bibliography

- [1] Adela Brigid, Nicholas R. A. Symons, Omar Faiz, Chris Fraser, Susan K. Clark, and Robin H. Kennedy. A systematic review regarding the feasibility and safety of endoscopic full thickness resection (eftr) for colonic lesions. *Surgical Endoscopy*, 27(10):3520–3529, 2013. ISSN 1432-2218. doi: 10.1007/s00464-013-2946-z. URL <http://dx.doi.org/10.1007/s00464-013-2946-z>. 4
- [2] Caroline E Bryson and D Caleb Rucker. Toward parallel continuum manipulators. In *Robotics and Automation (ICRA), 2014 IEEE International Conference on*, pages 778–785. IEEE, 2014. 47
- [3] E Clif Burdette, D Caleb Rucker, Punit Prakash, Chris J Diederich, Jordan M Croom, Clyde Clarke, Philipp Stolka, Titania Juang, Emad M Boctor, and Robert J Webster III. The acusitt ultrasonic ablator: the first steerable needle with an integrated interventional tool. In *SPIE Med. Imaging*, volume 7629, page 76290V, 2010. 3
- [4] Jessica Burgner, D Caleb Rucker, Hunter B Gilbert, Philip J Swaney, Paul T Russell, Kyle D Weaver, and Robert J Webster. A telerobotic system for transnasal surgery. *IEEE/ASME Transactions on Mechatronics*, 19(3):996–1006, 2014. 3
- [5] Jessica Burgner-Kahrs, D Caleb Rucker, and Howie Choset. Continuum robots for medical applications: A survey. *IEEE Transactions on Robotics*, 31(6):1261–1280, 2015. 2
- [6] Pierre E Dupont, Jesse Lock, Brandon Itkowitz, and Evan Butler. Design and control of concentric-tube robots. *IEEE Transactions on Robotics*, 26(2):209–225, 2010. 8
- [7] Johnathan A Engh, Davneet S Minhas, Douglas Kondziolka, and Cameron N Riviere. Percutaneous intracerebral navigation by duty-cycled spinning of flexible bevel-tipped needles. *Neurosurgery*, 67(4):1117–1123, 2010. 3
- [8] Roger E Goldman, Andrea Bajo, Lara S MacLachlan, Ryan Pickens, S Duke Herrell, and Nabil Simaan. Design and performance evaluation of a minimally invasive telerobotic platform for transurethral surveillance and intervention. *IEEE transactions on biomedical engineering*, 60(4):918–925, 2013. 3

- [9] Jose G Guillem, Philip B Paty, and Alfred M Cohen. Surgical treatment of colorectal cancer. *CA: a cancer journal for clinicians*, 47(2):113–128, 1997. 5
- [10] Junhyoung Ha and Pierre E Dupont. Designing stable concentric tube robots using piecewise straight tubes. *IEEE Robotics and Automation Letters*, 2(1):298–304, 2017. 14
- [11] Keiichi Ikeda, C. Alexander Mosse, Per-Ola Park, Annette Fritscher-Ravens, Maria Bergstrm, Tim Mills, Hisao Tajiri, and C. Paul Swain. Endoscopic full-thickness resection: circumferential cutting method. *Gastrointestinal Endoscopy*, 64(1):82 – 89, 2006. ISSN 0016-5107. doi: <http://dx.doi.org/10.1016/j.gie.2005.12.039>. URL <http://www.sciencedirect.com/science/article/pii/S001651070600143X>. 4
- [12] L Joskowicz, R Shamir, Z Israel, Y Shoshan, and M Shoham. Renaissance robotic system for keyhole cranial neurosurgery: in-vitro accuracy study. In *Proceedings of the Simposio Mexicano en Ciruga Asistida por Computadora y Procesamiento de Imgenes Mdicas (MexCAS11)*, 2011. 1
- [13] Tugrul T Kararli. Comparison of the gastrointestinal anatomy, physiology, and biochemistry of humans and commonly used laboratory animals. *Biopharmaceutics & drug disposition*, 16(5):351–380, 1995. 5
- [14] S Kiriya, Y Saito, S Yamamoto, R Soetikno, T Matsuda, T Nakajima, and H Kuwano. Comparison of endoscopic submucosal dissection with laparoscopic-assisted colorectal surgery for early-stage colorectal cancer: a retrospective analysis. *Endoscopy*, 44(11):1024–1030, November 2012. ISSN 0013-726X. doi: 10.1055/s-0032-1310259. URL <http://dx.doi.org/10.1055/s-0032-1310259>. 4
- [15] Michael Kranzfelder, Armin Schneider, Adam Fiolka, Sebastian Koller, Dirk Wilhelm, Silvano Reiser, Alexander Meining, and Hubertus Feussner. What do we really need? visions of an ideal human-machine interface for notes mechatronic support systems from the view of surgeons, gastroenterologists, and medical engineers. *Surgical Innovation*, page 1553350614550720, 2014. ISSN 1553-3506. 4

- [16] D. Y. Lee, J. Kim, J. S. Kim, C. Baek, G. Noh, D. N. Kim, K. Kim, S. Kang, and K. J. Cho. Anisotropic patterning to reduce instability of concentric-tube robots. *IEEE Transactions on Robotics*, 31(6):1311–1323, Dec 2015. ISSN 1552-3098. doi: 10.1109/TRO.2015.2481283. 29
- [17] A.J. Madhani and J.K. Salisbury. Articulated surgical instrument for performing minimally invasive surgery with enhanced dexterity and sensitivity, August 11 1998. URL <https://www.google.com/patents/US5792135>. US Patent 5,792,135. 1
- [18] Paul S Morgan, Timothy Carter, Stephen Davis, Arsalan Sepehri, Jonathan Punt, Paul Byrne, Alan Moody, and Patrick Finlay. The application accuracy of the pathfinder neurosurgical robot. In *International congress series*, volume 1256, pages 561–567. Elsevier, 2003. 1
- [19] Richard M Murray, Zexiang Li, and S Shankar Sastry. *A Mathematical Introduction to Robotic Manipulation*, volume 29. 1994. ISBN 9780849379819. doi: 10.1.1.169.3957. URL <http://scholar.google.com/scholar?hl=en{%&}btnG=Search{%&}q=intitle:A+Mathematical+Introduction+to+Robotic+Manipulation{%#}0>. 11, 40
- [20] Kaitlin Oliver-Butler, Zane H Epps, and Daniel Caleb Rucker. Concentric agonist-antagonist robots for minimally invasive surgeries. In *SPIE Medical Imaging*, pages 1013511–1013511. International Society for Optics and Photonics, 2017. 15, 16, 17
- [21] Andrew L Orekhov, Caroline B Black, John Till, Scotty Chung, and D Caleb Rucker. Analysis and validation of a teleoperated surgical parallel continuum manipulator. *IEEE Robotics and Automation Letters*, 1(2):828–835, 2016. 47
- [22] Gottumukkala S. Raju, Advitya Malhotra, and Ijaz Ahmed. Colonoscopic full-thickness resection of the colon in a porcine model as a prelude to endoscopic surgery of difficult colon polyps: a novel technique (with videos). *Gastrointestinal Endoscopy*, 70(1):159 – 165, 2009. ISSN 0016-5107. doi: <http://dx.doi.org/10.1016/j.gie.2009.02.022>. URL <http://www.sciencedirect.com/science/article/pii/S0016510709004210>. 4

- [23] Jose M Ramirez, Vicente Aguilera, Jose A Gracia, Javier Ortego, Pilar Escudero, Javier Valencia, Ricardo Esco, and Mariano Martinez. Local full-thickness excision as first line treatment for sessile rectal adenomas: long-term results. *Annals of surgery*, 249(2): 225–228, 2009. 4
- [24] Vivek Y Reddy, Petr Neuzil, Zachary J Malchano, Ragu Vijaykumar, Ricardo Cury, Suhny Abbata, Jiri Weichet, Christina D McPherson, and Jeremy N Ruskin. View-synchronized robotic image-guided therapy for atrial fibrillation ablation. *Circulation*, 115(21):2705–2714, 2007. 1
- [25] D Caleb Rucker, Bryan A Jones, and Robert J Webster III. A geometrically exact model for externally loaded concentric-tube continuum robots. *IEEE Transactions on Robotics*, 26(5):769–780, 2010. 9, 11
- [26] D Caleb Rucker, Robert J Webster, Gregory S Chirikjian, and Noah J Cowan. Equilibrium conformations of concentric-tube continuum robots. *The International journal of robotics research*, 2010. 8
- [27] Patrick Sears and Pierre Dupont. A steerable needle technology using curved concentric tubes. *IEEE International Conference on Intelligent Robots and Systems*, pages 2850–2856, 2006. doi: 10.1109/IROS.2006.282072. 7
- [28] Kazuki Sumiyama and Christopher J. Gostout. Novel techniques and instrumentation for emr, esd, and full-thickness endoscopic luminal resection. *Gastrointestinal Endoscopy Clinics of North America*, 17(3):471 – 485, 2007. ISSN 1052-5157. doi: <http://dx.doi.org/10.1016/j.giec.2007.05.009>. URL <http://www.sciencedirect.com/science/article/pii/S1052515707000438>. Endosurgery. 4
- [29] Intuitive Surgical. Clinical evidence. Webpage, 2017. URL <https://www.intuitivesurgical.com/company/clinical-evidence/>. 1
- [30] Philip J Swaney, Peter A York, Hunter B Gilbert, Jessica Burgner-Kahrs, and Robert J Webster. Design, fabrication, and testing of a needle-sized wrist for surgical instruments. *Journal of medical devices*, 11(1):014501, 2017. 15

- [31] Shyam Varadarajulu, Subhas Banerjee, Bradley A Barth, David J Desilets, Vivek Kaul, Sripathi R Kethu, Marcos C Pedrosa, Patrick R Pfau, Jeffrey L Tokar, Amy Wang, et al. Gi endoscopes. *Gastrointestinal endoscopy*, 74(1):1–6, 2011. [5](#)
- [32] Charles W Wampler. Manipulator inverse kinematic solutions based on vector formulations and damped least-squares methods. *IEEE Transactions on Systems, Man, and Cybernetics*, 16(1):93–101, 1986. [40](#)
- [33] Robert J. Webster, Allison M. Okamura, and Noah J. Cowan. Toward active cannulas: Miniature snake-like surgical robots. *IEEE International Conference on Intelligent Robots and Systems*, pages 2857–2863, 2006. doi: 10.1109/IROS.2006.282073. [7](#)
- [34] Robert J. Webster, Joseph M. Romano, and Noah J. Cowan. Mechanics of precurved-tube continuum robots. *IEEE Transactions on Robotics*, 25(1):67–78, 2009. ISSN 15523098. doi: 10.1109/TRO.2008.2006868. [7](#)
- [35] Robert J Webster III and Bryan A Jones. Design and kinematic modeling of constant curvature continuum robots: A review. *The International Journal of Robotics Research*, 29(13):1661–1683, 2010. [17](#)
- [36] Meidong Xu, Xiao-Yun Wang, Ping-Hong Zhou, Quan-Lin Li, Yiqun Zhang, Yunshi Zhong, Weifeng Chen, Lili Ma, S Ishaq, Wenzheng Qin, et al. Endoscopic full-thickness resection of colonic submucosal tumors originating from the muscularis propria: an evolving therapeutic strategy. *Endoscopy*, 45(09):770–773, 2013. [4](#)
- [37] Peter A York, Philip J Swaney, Hunter B Gilbert, and Robert J Webster. A wrist for needle-sized surgical robots. In *Robotics and Automation (ICRA), 2015 IEEE International Conference on*, pages 1776–1781. IEEE, 2015. [15](#)

Vita

Ryan Ponten was raised in Bellevue, WA, by his parents Byron and Diana Ponten and along with his brother Austin. After graduating Newport High School in 2010, he attended the University of Washington where he met his wife Kristine and began a Bachelor of Science degree in Mechanical Engineering. He married Kristine in the summer of 2013 between his junior and senior year, and together they continued their pursuit of higher learning. During his senior year, he enjoyed participating in a mechatronics option program, which ultimately led to his pursuit of graduate work in robotics. Immediately following his graduation in 2014 from the University of Washington, Ryan took a job at Measurement Technology NW as Mechanical/Electrical Technician. After a year of working there, he and Kristine moved to Tennessee to begin an exciting chapter in their lives. Ryan began graduate school at the University of Tennessee and was accepted as a graduate research assistant at the REACH Lab. He graduated with a Masters of Science in Mechanical Engineering in the summer of 2017. Ryan is pursuing a career in medical device engineering back home in Seattle, WA.